IEEE Photonics Journal
An IEEE Photonics Society Publication

Channel Capacity of Wavelength Division Multiplexing-Based Brillouin Optical Time Domain Sensors

Volume 10, Number 1, February 2018

Zelin Zhang
Yuangang Lu, ***Member, IEEE***
Yunqin Zhao

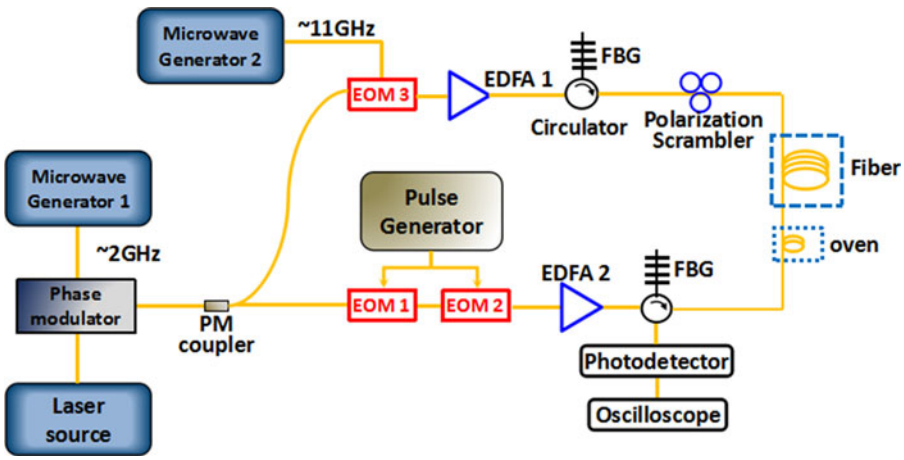

DOI: 10.1109/JPHOT.2018.2795658
1943-0655 © 2018 IEEE

IEEE photonics SOCIETY

IEEE

Channel Capacity of Wavelength Division Multiplexing-Based Brillouin Optical Time Domain Sensors

Zelin Zhang, Yuangang Lu, *Member, IEEE*, and Yunqin Zhao

Department of Applied Physics, College of Science, Nanjing University of Aeronautics and Astronautics, Nanjing 211106, China

DOI:10.1109/JPHOT.2018.2795658

Manuscript received November 13, 2017; revised January 15, 2018; accepted January 16, 2018. Date of publication January 23, 2018; date of current version February 7, 2018. This work was supported in part by National Natural Science Foundation of China (No. 61377086), in part by the Aerospace Science Foundation of China (2016ZD52042), in part by the Suzhou Application Research Program (No. SYG201546), and in part by the Foundation of Graduate Innovation Center in NUAA (No. Kfjj20170801).
Corresponding author: Yuangang Lu (e-mail: luyg@nuaa.edu.cn).

Abstract: We propose and demonstrate a novel WDM-based Brillouin optical time domain analysis (BOTDA) sensor using Brillouin loss configuration, and theoretically analyze channel capacity of WDM-based brillouin optical time domain reflectometry (BOTDR) and BOTDA sensors by considering the fiber dispersion and nonlinear effects in sensing fibers. A three-wavelength WDM-based BOTDA senor is experimentally validated in the distributed temperature measurement of a 23-km-long standard telecom fiber (SMF-28), demonstrating an electrical signal-to-noise ratio enhancement of 9.2 dB. The numerical calculation results of the channel capacity of WDM-based Brillouin optical time domain sensors show that, when compared with the conventional single-wavelength BOTDR and BOTDA sensors, 11-wavelength BOTDR and BOTDA sensor using large effective area fiber can respectively achieve 8.4 and 20.8 dB signal-noise-ratio improvement (SNRI), and 7-wavelength BOTDR and BOTDA sensor using SMF-28 can respectively achieve 7.2 B and 16.9 dB SNRI without evident spatial resolution degradation and nonlinear impairment.

Index Terms: Fiber sensing, WDM, BOTDR, BOTDA, nonlinear effects, dispersion.

1. Introduction

Over the past two decades, many types of Brillouin scattering based optical fiber sensors have been proposed for distributed simultaneous strain and temperature or single parameter monitoring [1]–[3]. These sensors can be classified into spontaneous and simulated Brillouin scattering-based sensors [4]–[9]. Brillouin Optical Time Domain Reflectometry (BOTDR) and Brillouin Optical Time Domain Analysis (BOTDA) are two time-domain based sensing techniques that are corresponding to spontaneous and simulated Brillouin scattering respectively, and both can be effectively used in structure monitoring field [1]–[3]. The signal-noise-ratio (SNR) of distributed sensing systems, which determines the dynamic range and measurement accuracy of the sensing systems, is one of the most important parameters for BOTDR and BOTDA systems. To improve the SNR of BOTDR and BOTDA sensors, many effective methods have been proposed, such as Er-doped fiber amplifier (EDFA) [2], sweep-free distributed Briilouin time-domain analyzer (SF-BOTDA) [10], coherent detection [4], Raman amplification [5], [11], vector SBS and frequency-agile technique

[12], self-heterodyne detection [13], time-division multiplexing [14], frequency-code multiplexing [15], combining frequency division multiplexing and in-line EDFAs [16], differential Brillouin gain [17], frequency-domain comb using multiple pump signals [18], and time and frequency pump-probe multiplexing [19]. Recently, we have proposed a Wavelength Division Multiplexing (WDM) based BOTDR sensor [20], where the probe pulse contains multiple wavelengths with small equal-wavelength spacing, which has been verified to improve the SNR of the BOTDR sensors. More recently, a 3-wavelength WDM-based BOTDA sensor using Brillouin gain mechanism is proposed to improve the SNR of the BOTDA system effectively [21]. In fact, when *N* pairs of light waves with small equal-wavelength spacing propagate in long optical fiber, the Group Velocity Dispersion (GVD) and severe nonlinear effects such as Self-Phase Modulation (SPM), Cross-Phase Modulation (XPM), Four-Wave Mixing (FWM) and modulation instability(MI) may be generated, and thus cause spatial resolution deterioration and SNR degradation. By utilizing the frequency division multiplexing with different time delay in time domain and unequal frequency spacing [19], the detrimental nonlinear effects can be effectively eliminated. However, for WDM-based systems, which are simpler and more efficient systems without the use of non-synchronous pulses and delayed signal traces reconstruction, the multiple beams are injected in the sensing fiber synchronously. Therefore, the system impairments and its corresponding channel capacity of WDM-based system should be considered. Unfortunately, there is no such analysis available in the literature.

In this paper, firstly we propose a new WDM-based BOTDA sensor utilizing Brillouin loss configuration that is considered to be used to achieve longer sensing length [2]. The scheme of the WDM-based BOTDA is simpler and efficient, compared with the combining time and frequency multiplexing method where the pulses must be non-synchronous to allow higher power and the delayed signal traces also require reconstruction. When compared with other SNR improvement (SNRI) approaches, the high SNRI, fast measurement speed and simple detection scheme can be maintained in the proposed method without using complex coding techniques and extra optical amplifiers. Different from the work of time and frequency pump-probe multiplexing, in the proposed WDM-based BOTDA using Brillouin loss, the *N* pump-probe pairs are injected synchronously with simple structure and signal processing. We describe the principles of the new WDM-based BOTDA system and the WDM-based BOTDR system [20], and analyze the SNR improvement in the two systems. The SNR enhancement is related with wavelength number (channel number in WDM-based system). Especially, the channel capacity of WDM-based Brillouin Optical Time Domain sensors are limited by the fiber dispersion and nonlinear effects. Therefore, taking two typical fibers, standard telecom fiber (SMF-28) and Large Effective Area Fiber (LEAF) as examples, we theoretically analyze the sensing systems impairment imposed by fiber dispersion and nonlinear effects such as SPM, XPM, FWM and MI. Considering the dispersion and nonlinear effects in sensing fibers, appropriate channel spacing, channel capacity and relevant parameters are theoretically obtained for the WDM-based BOTDR and BOTDA systems, which can achieve large SNR enhancement without evident spatial resolution deterioration compared with conventional single-wavelength systems. The calculation model related dispersion and nonlinear effects in *N*-wavelength WDM-based sensing systems can be of significant value in the search for suitable sensing fibers and provides a guide for designing WDM-based BOTDR and BOTDA sensors with high SNR.

2. WDM-Based BOTDA Sensor Using Brillouin Loss

Different from the WDM-based BOTDA system using Brillouin gain [21], the schematic diagram of WDM-based BOTDA system using Brillouin loss is displayed in Fig. 1. The multi-wavelength continuous pump and pulsed probe waves, whose frequencies are respectively. $\nu_1 + \nu_S, \nu_1 + \Delta\nu + \nu_S, \ldots, \nu_1 + (N-1)\Delta\nu + \nu_S$ and $\nu_1, \nu_1 + \Delta\nu, \ldots, \nu_1 + (N-1)\Delta\nu$, counter-propagate in the fiber. Likewise, the $\Delta\nu$ is frequency spacing, and the ν_S is pump-probe frequency differences, which is equivalent to Brillouin frequency shift. The *N* equal-spacing wavelength CW can be generated conveniently by multi-frequency phase modulation [22] or cascaded intensity and phase modulation [23], [24]. It should be noted that the maximum peak power of each pulse should be less than the critical power of modulation instability (MI) [25], as the MI turns out to be the dominant nonlinear

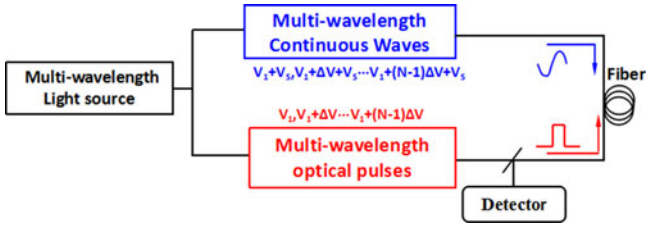

Fig. 1. Schematic diagram of WDM-based BOTDA sensor using Brillouin loss.

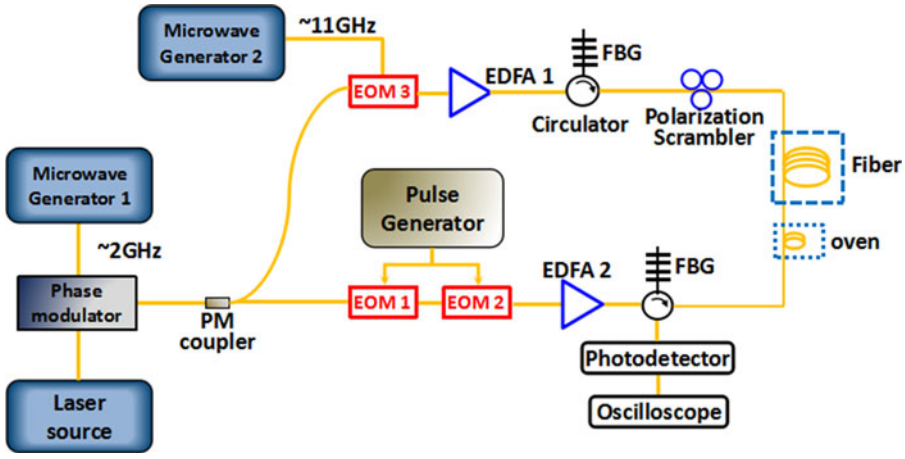

Fig. 2. Schematic diagram of a 3-wavelength BOTDA sensor using Brillouin loss.

limitation and it has the lowest critical power [26]. And the power of the CW should be selected to maintain low Brillouin gain with relatively high SNR without unacceptable excess amplification [2], [26].

Each pair of pump-probe waves interacts through SBS process independently and the photodetector directly detects the power of the multi-wavelength continuous waves transmitted through the sensing fiber. Just like the single-wavelength BOTDA system, what to be measured is the power transfer between probe and pump, and the transferred power corresponding to frequency difference composes the Brillouin loss spectrum. The quantity of power transfer, therefore, is significant to the BOTDA sensor's performance such as the SNR and the sensing range. More transferred power can generate higher SNR. Therefore, if one uses multiple pairs of probes and pumps whose frequency differences are equal to the BFS of the sensing fiber, the maximum SBS attenuation (or SBS amplification in SBS gain-based system) will occur synchronously and independently for these pairs and more power transfer can be realized, and thus a higher SNR can be achieved. In the following of the paper, when we mention the WDM-based BOTDA sensor, we shall consider only WDM-based BOTDA sensor using Brillouin loss. The results corresponding to the WDM-based BOTDA sensor using Brillouin gain can be obtained by following the methods described in the following sections.

A proof-of-concept experimental setup of a *N*-wavelength BOTDA sensor based on Brillouin loss is shown in Fig. 2, where a 3-wavelength BOTDA sensor is implemented. The light source is a 1549.35 nm single-wavelength semiconductor laser (Its frequency is denoted by ν_0) with linewidth 500 kHz and output power of 60 mW. And it was modulated by a phase modulator to obtain multi-wavelength waves with equal power. Restricted by the output amplitude and frequency of the Microwave generator1 in our lab, the available waves we could obtain were three wavelength light waves with an interval of 0.016 nm corresponding to a frequency spacing of 2 GHz. The three waves were divided into two beams. One was modulated to probe pulse by two cascade EOMs (EOM1 and EOM2) for the purpose of high extinction ratio (50 dB), while the other beam was

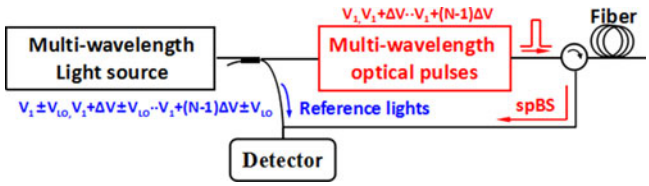

Fig. 3. Schematic diagram of WDM-based BOTDR sensor.

modulated by EOM3 to generate frequency shifted CW. Since the light wave generated by the EOM has two side bands, a filtering unit consisting of a fiber Bragg grating (FBG) and a circulator were used to get rid of the down-shifted side bands and the amplified spontaneous emission of the EDFA1. The 3 dB bandwidth of the two FBG filters is 0.1 nm. Thus, the frequencies of the three-wavelength CW injected in the sensing fiber are $\nu_0 + 9$ GHz, $\nu_0 + 11$ GHz and $\nu_0 + 13$ GHz, respectively. And the corresponding frequencies of the three-wavelength pulses are $\nu_0 - 2$ GHz, ν_0 and $\nu_0 + 2$ GHz, respectively. The polarization scrambler (General Photonics, scrambling frequency is 10 kHz) is used to eliminate the impairment to SBS induced by polarization state change. The three-wavelength pulses and three-wavelength CWs counter-propagated in the SMF-28 fiber, and the three-wavelength CW was detected by a 350 MHz bandwidth photodetector (PD). The high speed oscillator with 1 GHz bandwidth is used to acquire the time domain signal. The 45 m fiber at the far end of a 23.36 km SMF-28 sensing fiber was heated to 60 °C, while the rest of the fiber was at a room temperature of 19 °C. It should be noted that in a WDM-based BOTDA sensor, the bandwidth of the PD should be less than the frequency spacing to avoid the undesired beating between Rayleigh scattering of the pulses.

In the experiment the pulse width T_{in} was 50 ns, the peak power was P_{in} 64 mW and the CW power P_{CW} was 0.1 mW. The P_{in} was selected to provide sufficient signal while avoiding the detrimental MI [26] and reducing the Rayleigh backscattering of the probe pulses. In this case, the corresponding critical power of MI can be calculated as 116 mW [25]. Although the power P_{CW} was larger than the maximum CW power (0.034 mW) which is defined as the power that will cause the excess amplification of the pulses with a depletion factor of -0.2 in the worst situation [27], the BFS measurement error due to the excess amplification was negligible because the temperature difference between the long uniform unheated section and the 45 m, uniform heated section was as large as 41 °C. For comparison, another experiment using single-wavelength BOTDA sensor was also performed. In this case, the phase modulator and Microwave Generator1 were both removed, and the power of single-wavelength light wave was same as that of each three-wavelength light waves.

3. SNR Improvement in WDM-Based BOTDR and BOTDA Systems

In order to facilitate comparing the performance of the WDM-based BOTDR system [20] and the new WDM-based BOTDA system using Brillouin loss, we give a brief description about the WDM-based BOTDR system. The Fig. 3 shows the configuration of the WDM-based BOTDR system, which based on multi-wavelength coherent detection [20]. The multi-wavelength pulsed probe waves, whose frequencies are $\nu_1, \nu_1 + \Delta\nu, \ldots, \nu_1 + (N-1)\Delta\nu$, propagate in the fiber. The $\Delta\nu$ is frequency spacing and N is wavelength number. Each pulsed probe waves can interact with sensing fiber generating backscattering light with Brillouin frequency shift. The stokes and anti-stokes Brillouin scattering light waves of the multiple wavelengths beat with the corresponding local reference continuous wave(CW) with frequencies of $\nu_1 \pm \nu_{LO}, \nu_1 + \Delta\nu \pm \nu_{LO}, \ldots, \nu_1 + (N-1)\Delta\nu \pm \nu_{LO}$. The ν_{LO} is the frequency difference between the probe lights and their corresponding local reference lights.

To facilitate comparison between the N-wavelength sensors and single-wavelength ones, the powers of different probe and pump pairs are adjusted to equal in N-wavelength sensor. As that shown in [20], the SNR of the N-wavelength BOTDR sensor in terms of electrical signal-to-noise

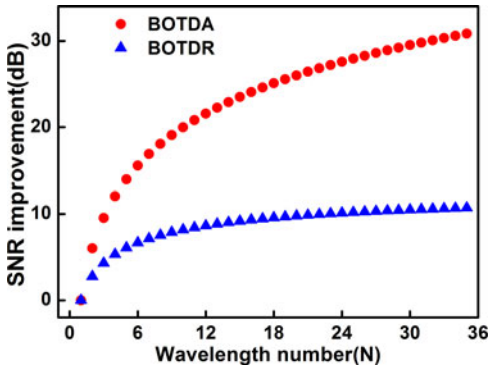

Fig. 4. SNR enhancement of system versus wavelength number in WDM-based BOTDR and BOTDA systems.

power ratio can be expressed as

$$SNR_N(z) = \frac{2R^2 N P_B(z) P_{LO}}{4kTB/R_L + 2qRN P_{LO} B + \langle i^2_{E-noise} \rangle} \tag{1}$$

The first term and second term among denominator represent thermal noise and shot noise caused by photo-detector, respectively. Furthermore, the third term denotes electrical noise existing in the signal receiving devices, such as Spectrum Analyzer. Where T denotes thermodynamic temperature, k denotes Boltzmann constant, R_L denotes load impedance, R denotes the photo-diode responsivity, and B denotes the electrical bandwidth of photo-diode.

The SNR of the N-wavelength BOTDA sensor using Brillouin loss can be expressed as

$$SNR_N(z) = \frac{(NR\Delta P_{CW}(z))^2}{2NqP_{CW}(z)RB + 4kTB/R_L + \langle i^2_{E-noise} \rangle + \langle i^2_{s-sp} \rangle} \tag{2}$$

where $\Delta P_{CW}(z)$ is the Brillouin gain signal power at location z along the fiber [28], and the power of the CW at z is $P_{CW}(z) = P_{CW}(L)\exp(-\alpha(L-z))$ where L is fiber length, α is fiber attenuation coefficient, and $Pcw(L) = Pcw$ is the input power of the CW source. The first and second items in the denominator are the mean-square shot noise power and thermal noise power of the detector, respectively. The third term denotes mean-square electrical noise power from other electrical devices in acquisition system, such as oscilloscope. The $\langle i^2_{s-sp} \rangle = 2P_{CW}(z) n_{sp} h\nu R^2 (G-1)B$ denotes the variance of signal-spontaneous noise [29], which depends on the amplified spontaneous emission (ASE) noise introduced by the EDFA [19]. n_{sp} is the spontaneous emission factor; while G is the optical amplifier gain [29]. Furthermore, the laser relative-intensity-noise (RIN), spontaneous-spontaneous photocurrent (sp-sp) and other noises are so week, which are relative to the electrical noise and signal-spontaneous noise, that we can neglect the impact induced by these noise. Thus the SNR improvement (SNRI) of the N-wavelength BOTDA sensor compared to a single-wavelength one is

$$SNRI(z) = \frac{N^2 (2NqP_{CW}(z)RB + 4kTB/R_L + \langle i^2_{E-noise} \rangle + \langle i^2_{s-sp} \rangle)}{2NqP_{CW}(z)RB + 4kTB/R_L + \langle i^2_{E-noise} \rangle + \langle i^2_{s-sp} \rangle} \tag{3}$$

By using the (1) and the (3), the SNRI in WDM-based BOTDR and BOTDA systems versus number of wavelength can be obtained, which is shown in Fig. 4. In the calculation, we use the parameters listed in Table 1, which are experimental parameters in our three-wavelength BOTDR sensor [20] and the aforementioned three-wavelength BOTDA sensor shown in Fig. 2. As it shown in Fig. 4, it is obvious that the introduction of WDM will greatly enhance the SNR of BOTDA and BOTDR sensors. When the wavelength number is larger than 10, the SNRI of the WDM-based BOTDA system will be larger than 20 dB, which indicates that using WDM method in BOTDA can potentially

TABLE 1
Main Parameters used to Calculate the SNRI of WDM-Based BOTDR and BOTDA Systems

	BOTDR	BOTDA
B (MHz)	800	350
T(K)	300	300
R(A/W)	1	1
$\langle i^2_{E-noise}\rangle (A^2)$	4.0×10^{-13}	7.9×10^{-11}
$R_L(\Omega)$	50	50
$\langle i^2_{s-sp}\rangle (A^2)$	—	9.1×10^{-13}

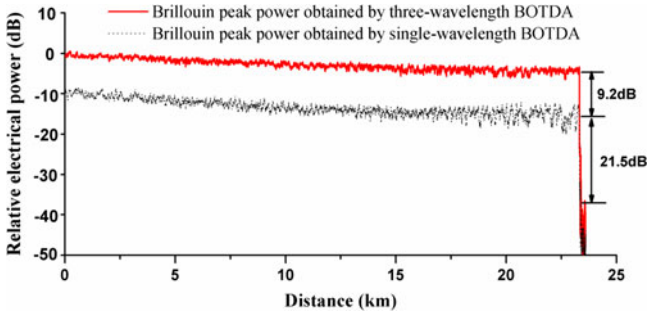

Fig. 5. The Brillouin peak power traces obtained by the three-wavelength and single-wavelength BOTDA sensors using Brillouin loss.

improve the sensing performance of the system greatly. It should be noted that the SNRI is limited by fiber dispersion and nonlinear effects which will be discussed in the following sections.

4. Experiment Results of BOTDA Sensors

Fig. 5 shows the Brillouin peak power traces obtained by the three-wavelength and single-wavelength BOTDA sensors using Brillouin loss. The two traces are shown in the form of relative electrical power. Because $\langle i^2_{E-noise}\rangle$ is absolutely dominant among noise sources and it is the same in three- and single-wavelength measurements, the noise floors at the end of the fiber for the three- and single-wavelength BOTDA sensors are almost the same, and the corresponding SNRs at the end of the fiber are 30.7 dB and 21.5 dB, respectively. As shown in Fig. 5, the peak electrical power obtained by the three-wavelength BOTDA sensor is 9.2 dB higher than that of single wavelength one, thus the electrical SNRI is 9.2 dB by the three-wavelength BOTDA sensor. The value agrees well with the calculated SNRI of 9.5 dB which was obtained by using the (3) and the values are listed in Table 1. The fluctuation along the two power trace is due to non-ideal polarization scrambling (low scrambling frequency of the polarization scrambler) and limited times of the repeated measurement (1000 times).

The distributed Brillouin frequency shift (BFS) measured by the three- and single-wavelength systems are shown in Fig. 6. The inset is the BFS of the entire fiber. Although the averaged BFS of the unheated section measured by the two systems are both 10865.2 MHz, the root-mean-square (RMS) errors of BFS obtained by three-wavelength and single-wavelength BOTDA sensors are 0.7 MHz and 1.2 MHz, respectively. The time interval were 2 minutes between the two RMS errors measurement of BFS at the same test temperature. The RMS errors of BFS for the 45 m heated

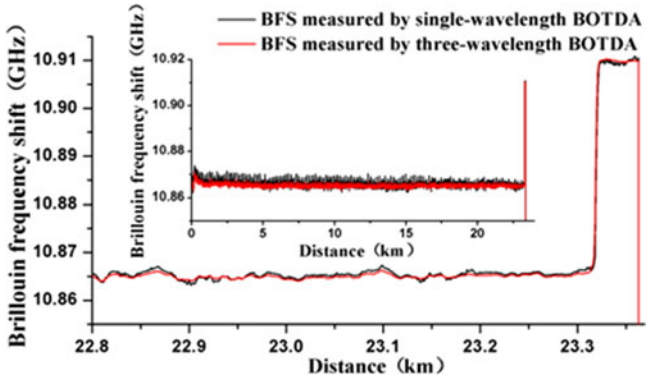

Fig. 6. The BFS obtained by the three-wavelength and single-wavelength BOTDA. The inset figure is the BFS curves of the entire fiber.

section are 0.2 MHz and 0.5 MHz, respectively, and thus the temperature measurement errors are, respectively, 0.2 °C and 0.5 °C (The calibration temperature coefficient of the fiber is 1.03 MHz/°C).

It is found that, in three-wavelength BOTDA using Brillouin loss, the SNR can achieve 9.2 dB improvement without observable small spatial resolution deterioration and nonlinear effects. Then the following question is that, provided the wavelength number is larger, whether the WDM-based systems can achieve higher SNR improvement without spatial resolution deterioration and nonlinear effects. Therefore, in the following sections the influences of chromatic dispersion and nonlinear effects on the WDM-based BOTDR and BOTDA sensors will be theoretically analyzed. And thus the suitable system parameters such as channel spacing, channel number and fiber type can be determined to achieve a large SNR enhancement in WDM-based BOTDR and BOTDA sensors.

5. Chromatic Dispersion Effect

Now we study the spatial resolution deterioration imposed by fiber chromatic dispersion in WDM-based BOTDR and BOTDA, and thus we can determine the suitable frequency ranges used in WDM-based systems. Although the pulse widths of the N pulses are the same when they injected into the fiber, they propagate with different group velocity, and thus result in a pulse broadening which will degrade the spatial resolution of sensing system. For the sensing fiber with length L, the deterioration of spatial resolution can be expressed as

$$\delta = (D \cdot L \cdot \Delta\lambda \cdot c) / 2n \tag{4}$$

where D is dispersion coefficient of sensing fiber, $\Delta\lambda$ denotes the wavelength range of incident lights, n denotes the effective refractive index around 1550 nm, and c is the light velocity in vacuum. We take two typical fibers, SMF-28 and LEAF as examples, and the corresponding parameters are shown in Table 2. When L is 50 km, and $\Delta\lambda$ for LEAF and SMF-28 are respectively 2 nm and 0.5 nm, the spatial resolution deterioration of LEAF and SMF-28 are respectively 0.04 m and 0.045 m, which can be acceptable for BOTDR and BOTDA sensors with a spatial resolution larger than 0.5 m. Accordingly, around 1550 nm the corresponding frequency range Δf for LEAF and SMF-28 are respectively 250 GHz and 62 GHz, which can be accepted in WDM-based BOTDR and BOTDA systems.

6. Nonlinear Effects

6.1 SPM and XPM Effects

The nonlinear effects SPM and XPM in WDM systems should be considered, as they may result in frequency chirp which causes pulse broadening and power fluctuation of probe light. In actual sensing systems, since one often obtain rectangular optical pulses with Gaussian rise and fall

TABLE 2
Main Parameters of LEAF and SMF-28

	LEAF	SMF-28
n (Refractive index)	1.4693	1.4679
D(Dispersion coefficient)	4 ps/(nm·km)	18 ps/(nm·km)
γ(Nonlinear coefficient)	1.535/(W·km)	1.063/(W·km)
g_B(Brillouin gain coefficient)	2×10^{-11} m/W	2×10^{-11} m/W
A_{eff}(Effective mode area)	72 μm^2	84 μm^2
α(Attenuation coefficient)	0.19 dB/km	0.20 dB/km
K($K = dn_g/d\lambda$)	1.2×10^{-6}/nm	5.4×10^{-6}/nm
β_2	-5.1 ps^2/km	-23 ps^2/km

time due to the influence of trailing and leading edge of the electrical pulse, the long optical pulse (pulse width T_{in}, peak power P_{in}) can be divided into a Gaussian pulse (pulse width T_0, peak power P_{in}) and a standard rectangular pulse (pulse width $T_{in} - T_0$, peak power P_{in}). The long standard rectangular pulse can be treated as the CW without considering SPM and XPM effects [30], so we will just consider the SPM and XPM among the N Gaussian pulses. In N-wavelength systems without initial time delay among probe pulses, similar to the case of two Gaussian pulses [30], the SPM- and XPM-induced frequency chirp for the i_{th} ($i = -M, \ldots, M$, $N = 2M + 1$) probe pulse which propagates to the position z is

$$\Delta\nu_i(T, z) = (\gamma_i z/\pi T_0)\, e^{-T^2/T_0^2} \times \left[P_i(z)\, T/T_0 + \sum_{j=-M, j\neq i}^{M} \left(2T - z d_{ij}\right) P_j(Z)\, /3T_0 \right] \tag{5}$$

where T is measured in a frame of reference moving with the pulse at the group velocity v_{gi} ($T = t - z/v_{gi}$) [30]. The γ_i is nonlinear coefficient in the i_{th} wavelength and can be regarded as a constant around 1550 nm. $P_i(z)$ is the peak power of the i_{th} Gaussian pulse at z and $d_{ij} = |v_{gj} - v_{gi}|/v_{gj}v_{gi}$. When all of N ($N = 2M + 1$) pulses have the same input peak power P_{in}, the maximum frequency chirp $\Delta\nu_{\max}$ will be located on $T = \sqrt{2}T_0/2$ and generated on the central probe wavelength because the total walk-off between this wavelength and other probe wavelengths are minimum.

For WDM-based BOTDR, the $\Delta\nu_{\max}$ without amplification can be expressed as

$$\Delta\nu_0\left(\frac{\sqrt{2}T_0}{2}, z\right) = \frac{\gamma z}{\pi T_0} e^{-\frac{1}{2}} P_{in} \times \left[\frac{\sqrt{2}(4M + 3)}{6} - \frac{\left(M^2 + M\right) zK\,\Delta\lambda}{3cT_0} \right] \tag{6}$$

However, for WDM-based BOTDA, considering the amplification caused by multiple CWs, and supposing the power of CW is P_{CW}, the $\Delta\nu_{\max}$ is

$$\Delta\nu_0\left(\frac{\sqrt{2}T_0}{2}, z\right) = \frac{\gamma z}{\pi T_0} e^{-\frac{1}{2}} P_{in} \exp\left(\eta_B g_B P_{cw} \frac{1 - \exp(-\alpha z)}{A_{eff}\alpha} - \alpha z\right) \times \left[\frac{\sqrt{2}(4M + 3)}{6} - \frac{\left(M^2 + M\right) zK\,\Delta\lambda}{3cT_0} \right] \tag{7}$$

where η_B is SBS efficiency and its value is 2/3 when pump and probe waves are completely random polarization [30]. The values of main parameters in (6) and (7) are shown in Table 2. And then, we can obtain the maximum pulse broadening $\Delta\tau_{\max} = \Delta\nu_{\max}|\beta_2|L$. where β_2 is GVD parameter, and the corresponding power fluctuation is $\delta P = (\Delta\tau_{\max})/(T_0 + \Delta\tau_{\max})$. When we use SMF-28 and LEAF as sensing fiber, and suppose $\Delta\lambda = 2$ nm, $T_{in} = 50$ ns, $T_0 = 4$ ns, $P_{in} = 64$ mW $P_{cw} = 0.1$ mW

TABLE 3
Pulse Broadening and Power Fluctuation when $N = 11, 21, 61$

		WDM-based BOTDR		WDM-based BOTDA	
Fiber type		**LEAF**	**SMF-28**	**LEAF**	**SMF-28**
$N = 11$	$\Delta\tau_{max}$	2.16*fs*	1.45*fs*	2.44*fs*	1.58*fs*
	δP	0.000054%	0.000036%	0.000061%	0.00004%
$N = 21$	$\Delta\tau_{max}$	4.03*fs*	2.70*fs*	4.56*fs*	2.93*fs*
	δP	0.000101%	0.000068%	0.000114%	0.000073%
$N = 61$	$\Delta\tau_{max}$	11.51*fs*	7.68*fs*	13.01*fs*	8.34*fs*
	δP	0.000288%	0.000192%	0.00032%	0.000208%

and $L = 50$ km, the pulse broadening and power fluctuation in WDM-based BOTDR and BOTDA systems can be obtained as shown in Table 3, where the N is selected as 11, 21 and 61, respectively. It is evident that the pulse broadening and power fluctuation are increased with the increase of the wavelength number N. For $N = 61$, the maximum pulse broadening $\Delta\tau_{\max}$ is 0.00032% and the maximum power fluctuation is 13.01 fs respectively. Hence, the system impairments imposed by SPM and XPM in WDM-based BOTDR and BOTDA sensors can be neglected by using suitable configuration of system parameters such as frequency spacing, wavelength number and input power.

6.2 FWM Effect

In the following, we will analysis FWM effects in WDM-based BOTDR and BOTDA systems. When three lights with frequencies f_s, f_p and f_q among N lights injected in fibers satisfy the frequency matching condition $f_{FWM} = f_s + f_p - f_q$, the total power of the new frequency f_{FWM} in WDM-based BOTDR generated through FWM at the location z can be expressed as [31], [32]

$$P_{FWM}(z) = \left| \sum_{\substack{s \neq p, s \neq q \\ s,p,q=1}}^{N} \eta\, d^2\, \gamma^2\, P_s\, P_p\, P_q \frac{\exp(-\alpha z)}{9} \times \left\{ \frac{\left[1 - \exp(-\alpha z)^2\right]}{\alpha^2} \right\} \right|^2 \tag{8}$$

where P_s, P_p and P_q denote the input power corresponding to frequencies f_s, f_p and f_q, respectively. In (8) d is the degeneracy factor, which can select $d = 1, 3$ and 6 [31]. And γ is the nonlinear coefficient, α is fiber attenuation coefficient and η is FWM efficiency which can be expressed as [31]

$$\eta = \alpha^2 / \left(\alpha^2 + \Delta\beta^2\right) \left\{ 1 + \left[4 \exp(-\alpha z) \sin^2 (\Delta\beta z/2) \right] \Big/ \left[1 - \exp(-\alpha z) \right]^2 \right. \tag{9}$$

where $\Delta\beta$ is phase-mismatch condition related to the frequency spacing among the multi-wavelengths.

Due to the amplification from continuous light in WDM-based BOTDA, the (8) is not able to describe the FWM power generated by N pulses in WDM-based BOTDA system. In a WDM-based BOTDA sensor, the new FWM component E_{FWM} propagating along sensing fiber can be described

as [33]

$$\frac{dE_{FWM}(z)}{dz} = -\frac{1}{2\alpha}E_{FWM}(z) + j\gamma E_s(z)E_p(z)E_q^*(z)e^{j\Delta\beta z} \tag{10}$$

where $E_s(z)$, $E_p(z)$ and $E_q(z)$ are the electric components corresponding to f_s, f_p and f_q, respectively. Through fiber attenuation and amplification by pump lights during SBS process, the light intensity I_s, I_p and I_q can be described as [34]

$$I_{s,p,q}(z) = I_{s,p,q}(0) \times \exp\left\{-\left[g\exp(-\alpha L)(e^{\alpha z}-1)I_{cw}(L)\right]/\alpha - \alpha z\right\} \tag{11}$$

where the L is the fiber length.

By using the relationship between light intensity and electric component $E_{s,p,q}(z) = \sqrt{I_{s,p,q}(z)A_{eff}}$ and boundary condition at $z = 0$. For the N injected pulses, the total FWM power in WDM-based BOTDA sensor generated at position z can be written as [35]

$$P_{FWM}(z) = \left| \sum_{\substack{s\neq p, s\neq q \\ s,p,q=1}}^{N} j\gamma E_s(0)E_p(0)E_q^*(0)\exp\left(-\frac{1}{2}\alpha z\right) \times \left\{ \int_0^z \exp\left[-\frac{3}{2}\beta(z) - \alpha z + j\Delta\beta z\right]dz + \frac{\tau}{240\pi}A_{eff}\right\}\right|^2 \tag{12}$$

where E_s, E_p and E_q denote the electric components corresponding to frequencies f_s, f_p and f_q, respectively. And $\beta(z)$ can be expressed as $\frac{g\cdot\exp(-\alpha L)(e^{\alpha z}-1)I_{cw}(L)}{\alpha}$; while the τ is pulse width. As mentioned before, limited by spatial resolution deterioration, the frequency range of incident lights for LEAF and SMF-28 are 250 GHz and 62 GHz, respectively. In the following discussion, the fiber length is still selected as 50 km, but a larger pulse peak power 100 mW is used to analysis the maximum FWM in WDM-based BOTDR and BOTDA system.

By use of the(8) and(12), the total FWM powers in all FWM frequency components versus frequency spacing are obtained in WDM-based BOTDR and WDM-based BOTDA, as shown in Fig. 7(a) and (b) respectively. It is clearly observed that the total FWM power is higher in small frequency spacing range than that in large frequency spacing range due to the large phase-mismatch within large frequency spacing range. Since the frequency range in LEAF is larger and thus it can contains more channels, the total FWM power in LEAF is higher than that in SMF-28 when the same frequency spacing is used in the two kind fibers. In Fig. 7(a), the peak FWM power for LEAF is 18.4 dBm(the corresponding frequency spacing is 5 GHz), and the ratios of total FWM power to total output power at 50 km fiber ends is 13.5%. Therefore, the evident FWM will degrade the SNR of the WDM-based system if there is no suitable configuration in channel frequency spacing. It should be noted that large channel frequency spacing, which corresponds to small FWM crosstalk, will cause the small channel capacity and thus result in low system SNR. In order to obtain a high SNRI, there should be a tradeoff between the channel frequency spacing and the FWM crosstalk.

For the N-wavelength pulses, during forward transmission process, due to the onset of FWM, the probe pulses continually transfer energy to new FWM frequency components. It may cause the power fluctuation among different pulse channel, which may results in nonuniform Brillouin gain in different channels and different sensing region. In order to maintain the uniformity of Brillouin gain, we consider that the total FWM power is .the acceptable impairment if it is less than 1% of the total output pulse power. The ratio of total FWM power to total output pulse power is defined as $P_{FWM}(L)/[N \cdot P(L)]$ ($P(L)$ is the output power of single pulse with fiber loss), and N are $\frac{250}{\Delta\upsilon}$ and $\frac{62}{\Delta\upsilon}$ ($\Delta\upsilon$ is the corresponding frequency spacing) for LEAF and SMF-28, respectively. As it shown in Fig. 7(a) and (b), we find that the total power fluctuation induced by FWM around -3 dBm is

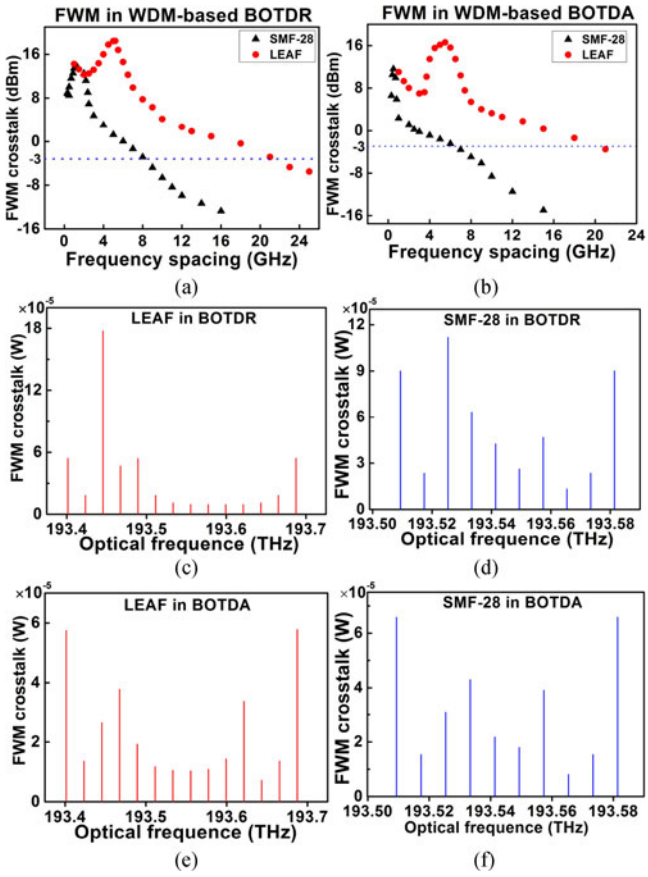

Fig. 7. (a) and Fig. 7(b) show the total FWM power versus frequency spacing in WDM-based BOTDR and BOTDA systems, respectively. Fig. 7(c) and Fig. 7(d) show the FWM spectrums of WDM-based BOTDR sensors using LEAF and SMF-28, respectively. Fig. 7(e) and Fig. 7(f) show the FWM spectrums of WDM-based BOTDA sensors using LEAF and SMF-28, respectively.

about 0.5% of the total output pulse power. In such situations, the power fluctuation of pulses due to FWM can be neglected. When the total FWM power is round -3 dBm, the corresponding frequency spacing are about 22 GHz and 8 GHz for LEAF and SMF-28, respectively. Thus we choose such frequency spacing, and the corresponding channel capacity in LEAF and SMF-28 are 11 and 7, respectively. In such cases, according to Fig. 4 the SNRI in 11-wavelength BOTDR and BOTDA sensor using LEAF are 8.4 dB and 20.8 dB, respectively. And the SNRI in 7-wavelength BOTDR and BOTDA sensor using SMF-28 are 7.2 dB and 16.9 dB, respectively.

The FWM power spectrums of WDM-based BOTDR and BOTDA systems using LEAF and SMF-28 are obtained, as shown in Fig. 7(c), (d), (e) and (f). In these figures, the maximum channel FWM powers are 0.18 mW, 0.11 mW, 0.058 mW and 0.08 mW, respectively. As it shown in Fig. 7(c), at the end of 50 km fiber, the maximum channel FWM power is 1.8% of the single wavelength output power for WDM-based BOTDR sensor using LEAF. And the total FWM powers are 0.45 mW, 0.39 mW, 0.46 mW and 0.37 mW, respectively. However, the ratios of total FWM power to output power at fiber ends for the four systems are 0.41%, 0.56%, 0.42% and 0.53%, respectively. Therefore, in such cases the FWM in WDM-based BOTDR and BOTDA systems can be neglected.

Now we consider whether the FWM crosstalk generated by N-wavelength CWs has influence on Brillouin gain signal in WDM-based BOTDA. The Brillouin gain signal power, $\Delta P_{CW}(z)$, can be obtained as that shown in [30]. The FWM crosstalk generated by CWs, $P_{FWM}(L)$ can be calculated by using (8). In the calculations, as mentioned above, the wavelength number N is 11 for LEAF, and the wavelength number N is 7 for SMF-28. As the frequency space $\Delta\nu$ for LEAF and SMF-28 are

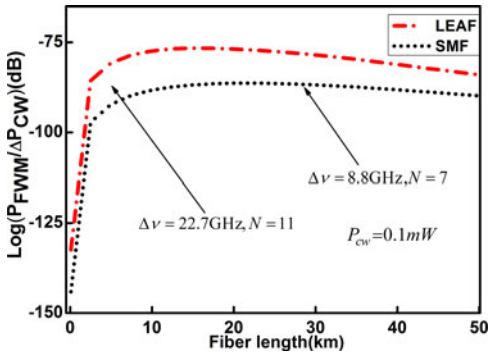

Fig. 8. The relative value between FWM crosstalk and Brillouin gain signal along the fiber.

respectively $\frac{250}{N}$ GHz and $\frac{62}{N}$ GHz, and the $\Delta\upsilon$ for the two kinds fiber are respectively 22.7 GHz and 8.8 GHz in this case. The relative value between FWM crosstalk and Brillouin gain signal along the fiber is shown in Fig. 8.

As it shown in the Fig. 8, for the fiber LEAF or SMF, the Brillouin gain is almost seven orders of magnitude larger than the FWM generated from CWs. The reason for the very low FWM is that the power of CWs is very weak (In the case the power is 0.1 mW). Hence the FWM generated from CWs can be neglected in WDM-based BOTDA. It should be noted that the FWM generated by forward transmission pulses will not directly affect the Brillouin gain. As mentioned above, when the total FWM power generated by pulses is less than 1% of the total output power. Because the transferred power from *N* pulses to FWM components is less than 1%, the corresponding power fluctuation of the Brillouin gain signal is also less than 1% [28]. Therefore, the FWM generated from pulses can be neglected in WDM-based BOTDA as well.

6.3 MI Effect

Furthermore, we also consider that modulation instability (MI) process may cause the impact for pulses and CWs in WDM-based BOTDA. Furthermore, we also consider the impact caused by the modulation instability (MI) of *N*-wavelength pulses and CWs in WDM-based BOTDA. Based on the work of [36], the power P_{MI} transferred from single pulse or CW to their MI sidebands can be expressed as

$$P_{MI} = \int_{-\nu_C}^{\nu_C} G_{MI}(\nu)\, S_n d\nu \tag{13}$$

where S_n denotes the power spectral density of the background noise, and $G_{MI}(\nu)$ is the spectral distribution of the modulation instability gain which can be expressed as [37]

$$G_{MI}(\nu) = 1 + \frac{\mathrm{Sin\,h}^2\left[2\gamma P_0 L\sqrt{\left(\frac{\nu}{\nu_C}\right)^2\left(1-\left(\frac{\nu}{\nu_C}\right)^2\right)}\right]}{2\left(\frac{\nu}{\nu_C}\right)^2\left[1-\left(\frac{\nu}{\nu_C}\right)^2\right]} \tag{14}$$

where P_0 is the original power of the pulses or CWs injected into fiber, and $\nu_C = \sqrt{4\gamma P_0/|\beta_2|}$ is the critical frequency of MI gain spectrum.

In *N*-wavelength WDM-based BOTDA systems, if $\nu_C \leq \Delta\upsilon$, the MI spectrum generated from each CW or pulse lightwave will not overlap, thus the P_{MI} within the critical frequency of certain wavelength can be calculated as the (13). For the cases of $\nu_C > \Delta\upsilon$, the MI spectrum generated from adjacent wavelength CW or pulse will be overlapped, and the overlapped factor can be defined as $\nu_C/\Delta\upsilon$ for simplifying calculation, if the MI spectrum can be considered approximately as a rectangle shape. Hence, in such cases the P_{MI} within the critical frequency of certain wavelength

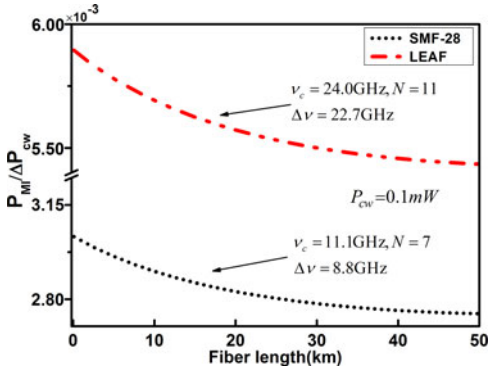

Fig. 9. The relative value between MI power of CWs and Brillouin gain signal along the fiber.

can be evaluated by

$$P_{MI} = \frac{\nu_C}{\Delta\upsilon} \int_{-\nu_C}^{\nu_C} G_{MI}(\nu) S_n d\nu \tag{15}$$

Now we firstly calculate the ratio of P_{MI} to ΔP_{CW} along the fiber to analyze the impact of MI crosstalk to Brillouin gain signal. In order to maintain the Brillouin gain at a suitable high level [25], we regard -135 dBm/Hz as the typical value of S_n [38]. When the power of CWs is 0.1 mW, the critical frequency ν_C for LEAF and SMF-28 are 1.7 GHz and 0.7 GHz, respectively. In our optimal wavelength configurations, the $\Delta\nu$ for LEAF and SMF-28 are respectively 22.7 GHz and 8.8 GHz, which are larger than the corresponding critical frequency. Therefore, we should use the (13) to evaluated the P_{MI}, and the ratio of P_{MI} to ΔP_{CW} can be obtained as that shown in Fig. 9. As it shown in the Fig. 9, for the fiber LEAF or SMF, the P_{MI} generated by CWs is about 3 orders of magnitude smaller than the Brillouin gain. The reason for the very low MI is that the power of CWs is very weak (in the case the power is 0.1 mW). Hence the MI generated from CWs can be neglected in WDM-based BOTDA.

Similar as the cases of the FWM generated by forward transmission pulses, the MI generated by forward transmission pulses will not directly affect the Brillouin gain. If the pulse power is 100 mW, the critical frequency ν_C for LEAF and SMF-28 are respectively 73.1 GHz and 30.6 GHz which are larger than the corresponding critical frequency. Thus the power fluctuation caused by pulses should be calculated by using (15). For LEAF and SMF-28, the transferred power from N pulses to MI sidebands is about 0.93% and 0.77% of the total output power. Since the transferred power from N pulses to MI components is less than 1%, the corresponding power fluctuation of the Brillouin gain signal is also less than 1% [28]. Therefore, the MI generated from pulses can be neglected in WDM-based BOTDA as well.

For the case of the WDM-based BOTDR, the FWM and MI can be generated from multiple forward transmitted pulses, too. However, what to be measured in BOTDR is the backscattering signal, thus the backscattering of the forward transmitted FWM and MI is so weak that can be neglected.

7. Conclusion

In conclusion, we propose and verify a new WDM-based BOTDA sensor utilizing Brillouin loss, and we theoretically analyzed channel capacity of WDM-based BOTDR and BOTDA systems by considering the fiber dispersion and nonlinear effects such as SPM, XPM, FWM and MI. A three-wavelength WDM-based BOTDA senor is experimentally validated in a 23 km-long SMF-28 distributed temperature measurement, where the SNR is 9.2 dB higher than that of single wavelength BOTDA sensor. Furthermore, we theoretically analyze the channel capacity of WDM-based Brillouin Optical Time Domain sensors. The numerical calculation results show that, provided we choose suitable system parameters such as channel spacing, channel number and fiber type, the

proposed WDM-based BOTDA and BOTDR systems are able to achieve large SNR enhancement without evident impairments imposed by fiber dispersion and nonlinearities. When compared with the conventional single-wavelength BOTDR and BOTDA systems, 11-wavelength BOTDR and BOTDA sensor using LEAF can respectively achieve 8.4 dB and 20.8 dB SNRI, and 7-wavelength BOTDR and BOTDA sensor using SMF-28 can respectively achieve 7.2 dB and 16.9 dB SNRI without evident spatial resolution degradation and nonlinear impairment.

References

[1] T. Horiguchi, K. Shimizu, T. Kurashima, M. Tateda, and Y. Koyamada, "Development of a distributed sensing technique using Brillouin scattering," *J. Lightw. Technol.*, vol. 13, no. 7, pp. 1296–1302, Jul. 1995.

[2] X. Bao and L. Chen, "Rent progress in Brillouin scattering based fiber sensors," *Sensor*, vol. 11, pp. 4152–4187, Nov. 2011.

[3] M. A. Soto and L. Thévenacez, "Modeling and evaluating the performance of Brillouin distributed optical fiber sensors," *Opt. Exp.*, vol. 21, no. 25, pp. 31347–31366, Dec. 2013.

[4] K. Shimizu, T. Horiguchi, Y. Koyamada, and T. Kurashima, "Coherent self-heterodyne Brillouin OTDR for measurement of Brillouin frequency shift distribution in optical fibers," *J. Lightw. Technol.*, vol. 12, no. 5, pp. 730–736, May 1994.

[5] Y. T. Cho, M. Alahbabi, M. J. Gunning, and T. P. Newson, "50-km single-ended spontaneous-Brillouin-based distributed-temperature sensor exploiting pulsed Raman amplification," *Opt. Lett.*, vol. 28, no. 18, pp. 1651–1653, Sep. 2003.

[6] K. Hotate and M. Tanaka, "Distributed fiber Brillouin strain sensing with 1 cm spatial resolution by correlation-cased continuous-wave technique," *IEEE Photon. Technol. Lett.*, vol. 14, no. 2, pp. 179–181, Feb. 2002.

[7] M. Nikl'es, L. Thévenaz, and P. Robert, "Simple distributed fiber sensor based on Brillouin gain spectrum analysis," *Opt. Lett.*, vol. 21, no. 10, pp. 758–760, May. 1996.

[8] X. Bao, D. J. Webb, and D. A. Jackson, "32-km distributed temperature sensor based on Brillouin loss in an optical fiber," *Opt. Lett.*, vol. 18, no. 18, pp. 1561–1563, Sep. 1993.

[9] D. Garus, K. Krebber, F. Schliep, and T. Gogolla, "Distributed sensing technique based on Brillouin optical-fiber frequency-domain analysis," *Opt. Lett.*, vol. 21, no. 17, pp. 1402–1404, Sep. 1996.

[10] A. Voskoboinik, O. F. Yilmaz, and A. W. Willner, "Sweep-free distributed Brillouin time-domain analyzer (SF-BOTDA)," *Opt. Exp.*, vol. 19, no. 26, pp. 842–847, Dec. 2011.

[11] X. Jia, Y. Rao, L. Chang, C. Zhang, and Z. Ran, "Enhanced sensing performance in long distance Brillouin optical time-domain analyzer based on Raman amplification: Theoretical and experimental investigation," *J. Lightw. Technol.*, vol. 28, no. 11, pp. 1624–1630, Apr. 2010.

[12] D. Zhou, Y. Dong, and B. Wang, "Slope-assisted BOTDA based on vector SBS and frequency-agile technique for wide-strain-range dynamic measurements," *Opt. Exp.*, vol. 25, no. 3, pp. 1889–1902, Feb. 2017.

[13] A. Zornoza, M. Sagues, and A. Loayssa, "Self-heterodyne detection for SNR improvement and distributed phase-shift measurements in BOTDA," *J. Lightw. Technol.*, vol. 30, no. 8, pp. 1066–1072, Apr. 2012.

[14] Y. Dong, L. Chen, and X. Bao, "Time-division multiplexing-based BOTDA over 100 km sensing length," *Opt. Lett.*, vol. 36, no. 2, pp. 277–279, Jan. 2011.

[15] C. Kito, F. Ito, H. Takahashi, and K. Toge, "Frequency-code multiplexed end reflection assisted Brillouin analysis for monitoring PONs," in *Proc. 39th Eur. Conf. Exhib. Opt. Commun.*, London, U.K., 2013, Paper We. 2. F. 3.

[16] Y. Dong, L. Chen, and X. Bao, "Extending the sensing range of Brillouin optical time-domain analysis combining frequency-division multiplexing and in-line EDFAs," *J. Lightw. Technol.*, vol. 30, no. 8, pp. 1161–1167, Oct. 2012.

[17] Y. Dong, X. Bao, and W. Li, "Differential Brillouin gain for improving the temperature accuracy and spatial resolution in a long-distance distributed fiber sensor," *Appl. Opt.*, vol. 48, no. 22, pp. 4297–4301, Aug. 2009.

[18] P. Chaube, B. G. Colpitts, and D. Jagannathan, "Distributed fiber-optic sensor for dynamic strain measurement," *IEEE Sensors J.*, vol. 8 no. 7, pp. 1067–1072, Jul. 2008.

[19] M. A. Soto, A. L. Ricchiuti, L. Zhang, D. Barrera, S. Slaes, and L. Thévenaz, "Time and frequency pump-probe multiplexing to enhance the signal response of Brillouin optical time-domain analyzers," *Opt. Exp.*, vol. 22, no. 23, pp. 28584–28595, Nov. 2015.

[20] C. Li, Y. Lu, and X. Zhang, "SNR enhancement in Brillouin optical time domain reflectometer using multi-wavelength coherent detection," *Electron. Lett.*, vol. 48, no. 18, pp. 1139–1141, Aug. 2012.

[21] N. Lalam, W. P. Ng, and X. Dai, "Employing wavelength diversity technique to enhance the Brillouin gain response in BOTDA system," in *Proc. Opt. Fiber Commun. Conf. Exhib.*, Anaheim, CA, USA, 2016, Paper M2D.4.

[22] Y. Liu, Z. Lv, Y. Dong, and Q. Li, "Research on stimulated Brillouin scattering suppression based on multi-frequency phase modulation," *Chin. Opt. Lett.*, vol. 7, no. 1, pp. 29–31, Jan. 2009.

[23] Y. Dou, H. Zhang, and M. Yao, "Generation of flat optical-frequency comb using cascaded intensity and phase modulators," *IEEE Photon. Technol. Lett.*, vol. 24, no. 9, pp. 727–729, Feb. 2012.

[24] R. Wu, V. R. Supradeepa, C. M. Long, D. E. Leaird, and A. M. Weiner, "Generation of very flat optical frequency combs from continuous-wave lasers using cascaded intensity and phase modulators driven by tailored radio frequency waveforms," *Opt. Lett.*, vol. 35, no. 19, pp. 3234–3236, Oct. 2010.

[25] M. Alem, M. A. Soto, and L. Thévenaz, "Analytical model and experimental Verification of the critical power for modulation instability in optical fibers," *Opt. Exp.*, vol. 23, no. 23, pp. 29514–29532, Nov. 2015.

[26] S. M. Foaleng and L. Thévenaz, "Impact of Raman scattering and modulation instability on the performances of Brillouin sensors," in *Proc. SPIE*, vol. 7753, 2011, pp. 77539V1–77539V4.

[27] L. Thévenaz, S. F. Mafang, and J. Lin, "Effect of pulse depletion in a Brillouin optical time-domain analysis system," *Opt. Exp.*, vol. 21, no. 12, pp. 14017–14035, Jun. 2013.

[28] T. Horiguchi and M. Tateda, "BOTDA-nondestructive measurement of single-mode optical fiber attenuation characteristics using brillouin interaction: Theory," *J. Lightw. Technol.*, vol. 7, no. 8, pp. 1170–1176, Aug. 1989.
[29] F. Jacobs, "Dependence of optical amplifier noise figure on relative-intensity-noise," *J. Lightw. Technol.*, vol. 13, no. 7, pp. 1461–1465, Jul. 1995.
[30] G. P. Agrawal, *Nonlinear Fiber Optics*, 4th ed. San Francisco, CA, USA: Academic, 2007.
[31] R. P. B. Shibata, and R. G. Waarts, "Phase-mismatch dependence of efficiency of wave generation through four-wave mixing in a single-mode optical fiber," *IEEE J. Quantum Electron.*, vol. QE-23, no. 7, pp. 1205–1210, Jul. 1987.
[32] F. Forghieri, R. W. Tkach, and A. R. Chraplyvy, "WDM system with unequally spaced channels," *J. Lightw. Technol.*, vol. 13, no. 5, pp. 897–899, May 1995.
[33] F. Di Pasquale, and F. Meli, "New Raman pump module for reducing pump-signal four-wave-mixing interaction in co-pumped distributed Raman amplifiers," *J. Lightw. Technol.*, vol. 21, no. 8, pp. 1742–1748, Aug. 2003.
[34] X. Bao, J. Dhliwayo, N. Heron, D. J. Webb, and D. A. Jackson, "Experimental and theoretical studies on a distributed temperature sensor based on Brillouin scattering," *J. Lightw. Technol.*, vol. 13, no. 7, pp. 1340–1348, Jul. 1995.
[35] S. Song *et al.*, "Intensity-dependent phase-matching effects on four-wave mixing in optical fibers," *J. Lightw. Technol.*, vol. 17, no. 11, pp. 2285–2289, Nov. 1999.
[36] M. Alem, M. A. Soto, and L. Thévenaz, "Modelling the depletion length induced by modulation instability in distributed optical fibre sensors," in *Proc. SPIE*, vol. 9157, 2014, pp. 91575S1–91575S4.
[37] M. A. Soto, M. Alem, W. Chen, and L. Thévenaz, "Mitigating modulation instability in Brillouin distributed fibre sensors," in *Proc. SPIE*, vol. 8794, 2013, pp. 87943J1–87943J4.
[38] E. Desurvire, *Erbium-Doped Fiber Amplifiers: Principles and Applications*. New York, NY, USA: Wiley, 1994.